AGU PUBLICATIONS

JGR

Journal of Geophysical Research: Planets

RESEARCH ARTICLE
10.1002/2016JE005215

Key Points:
- We found that bottom heated convection is incompatible with the observations of Sputnik Planum
- Volumetrically heated convection is a robust model for explaining the observed polygonal pattern
- Variations in surface temperature caused by variations in Pluto's orbit may be the source of heating

Supporting Information:
- Supporting Information S1
- Movie S1

Correspondence to:
K. Vilella and F. Deschamps,
vilella@earth.sinica.edu.tw;
frederic@earth.sinica.edu.tw

Citation:
Vilella, K., and F. Deschamps (2017), Thermal convection as a possible mechanism for the origin of polygonal structures on Pluto's surface, *J. Geophys. Res. Planets*, *122*, 1056–1076, doi:10.1002/2016JE005215.

Received 8 NOV 2016
Accepted 13 MAY 2017
Accepted article online 18 MAY 2017
Published online 27 MAY 2017

Thermal convection as a possible mechanism for the origin of polygonal structures on Pluto's surface

Kenny Vilella[1] and Frédéric Deschamps[1]

[1] Institute of Earth Sciences, Academia Sinica, Taipei, Taiwan

Abstract High-resolution pictures of Pluto's surface obtained by the *New Horizons* spacecraft revealed, among other surface features, a large nitrogen ice glacier informally named Sputnik Planitia. The surface of this glacier is separated into a network of polygonal cells with a wavelength of ~20–40 km. This network is similar to the convective patterns obtained under certain conditions by laboratory experiments, suggesting that it is the surface expression of thermal convection. Here we investigate the surface planform obtained for different convective systems in 3-D Cartesian geometry with different modes of heating and rheologies. We find that bottom heated systems, as assumed by previous studies, do not produce surface planforms consistent with the observed pattern. Alternatively, for a certain range of Rayleigh-Roberts number, Ra_H, a volumetrically heated system produces a surface planform similar to this pattern. We then combine scaling laws with values of Ra_H within its possible range to establish relationships between the critical parameters of Sputnik Planitia. In particular, our calculations indicate that the glacier thickness and the surface heat flux are in the ranges 2–10 km and 0.1–10 mW m^{-2}, respectively. However, a difficulty is to identify a proper source of internal heating. We propose that the long-term variations of surface temperature caused by variations in Pluto's orbit over millions of years produces secular cooling equivalent to internal heating. We find that this source of heating is sufficient to trigger thermal convection, but additional investigations are needed to determine under which conditions it can produce surface patterns similar to those of Sputnik Planitia.

1. Introduction

NASA's *New Horizons* spacecraft has operated the first flyby of the dwarf planet Pluto on 14 July 2015, providing an important source of information about this planet and its system [*Stern et al.*, 2015]. High-resolution pictures of Pluto's surface revealed a complex geology with a large diversity of terrains. One of them, informally named Sputnik Planitia, is a glacier extending several hundreds of kilometers across and mainly composed of nitrogen ices [*Cruikshank et al.*, 2015]. The unique character of Sputnik Planitia stems from the fact that its surface is separated into polygonal cells with ~20–40 km wavelength. Cell borders have a complex 2–3 km wide double-ditch structure, consisting of a rift, up to ~100 m deep, with a raised center. The centers of the polygonal cells are typically raised by ~50 m compared to their edges. These structures have been identified as a surface expression of thermal convection within the glacier [*Moore et al.*, 2016; *McKinnon et al.*, 2016; *Trowbridge et al.*, 2016]. Following this hypothesis, the rift separating the polygons would correspond to dynamic topography induced by downwellings.

Studies of Sputnik Planitia dynamics conducted so far have considered Rayleigh-Bénard convection, namely, a fluid with isothermal surface and base, the surface temperature being colder than the bottom one. In such a system, heat comes from the bottom and is transported to the top by upwellings, while downwellings entrain cold material from the subsurface to the interior. Laboratory experiments [*Whitehead and Parsons*, 1977; *White*, 1988] and numerical simulations [*Christensen and Harder*, 1991] showed that for a certain range of control parameters (including the Rayleigh number, which controls the vigor of convection) a polygonal pattern can be obtained when selecting a specific (imposed) initial temperature condition. Using appropriate rheology for nitrogen, *Moore et al.* [2016] and *McKinnon et al.* [2016] showed that Rayleigh-Benard convection may operate within Sputnik Planitia, provided that a heat flux of a few mW m^{-2} is available at its base. However, these calculations were conducted in 2-D Cartesian geometry, and 3-D experiments are required to verify that the surface planform of their convective system does exhibit a polygonal structure.

Convection may also operate in internally heated systems. Such systems are cooled from above, with no heat flux at their base. Only downwellings are generated, as a result of the growth of instabilities below the surface, and the upward motion consists only of return flow. Experiments of volumetrically heated convection predict the formation of a polygonal cell structure at the top of the system, usually referred to as a "sheet-like" structure [e.g., *Weinstein and Olson*, 1990; *Limare et al.*, 2015], similar to the one observed on Sputnik Planitia. Numerical simulations of *Vilella* [2015] have further shown that the sheet-like structure, required to explain the polygonal structure, is stable only for certain values of the Rayleigh-Roberts number. In addition, the temperature jump across the thermal boundary layer (TBL) and the thickness of this TBL are related to the Rayleigh-Roberts number. The surface planform therefore provides an original way to determine the internal structure of the convective system. For Sputnik Planitia, however, a difficulty is to identify a possible source of internal heating. Classical sources, i.e., radiogenic heating and tidal dissipation, can be ruled out. So far, volumetrically heated convection was therefore not considered as a possible mechanism describing Sputnik Planitia dynamics. Interestingly, variations of Pluto's orbit over millions of years induces changes in surface temperature [*Earle et al.*, 2017]. This would in turn produce secular cooling, which is strictly equivalent to volumetric heating [*Krishnamurti*, 1968; *Daly*, 1980; *Weinstein and Olson*, 1990], within Sputnik Planitia.

Here we first investigate the surface planform obtained for different convective systems with different modes of heating and rheologies. Numerical simulations performed for a bottom heated system operating either in an isoviscous fluid, sluggish-lid, or stagnant-lid regime predict a surface dynamic topography that disagrees with observations. Alternatively, a volumetric heated system gives a very good agreement with the surface of Sputnik Planitia. We suggest that volumetric heating may be caused by variations of Pluto's orbit [*Kinoshita and Nakai*, 1996] and verify that the variations of surface temperature caused by orbital variations are sufficient to trigger convection within Sputnik Planitia.

2. Sputnik Planitia Composition and Properties

Before *New Horizons*'s flyby, ground-based observations gave first insights of Pluto's surface composition [*Cruikshank et al.*, 2015]. These observations were based on near-infrared spectroscopy, which provides absorption spectra that can be interpreted in terms of molecular ices. Four main types of ices were detected: two major, N_2 and CH_4, and two minor, CO and C_2H_6. However, explaining Pluto's spectra is challenging and is limited by available experimental data. Pure ices components are not able to fully explain the observed spectra, and additional mixtures are required. Comparisons with results from laboratory experiments suggest that a low proportion of CH_4 is diluted in N_2 ice, and a low proportion of N_2 is diluted in CH_4 ice [*Prokhvatilov and Yantsevich*, 1983]. Another complexity is the likely heterogeneous spatial distribution of ices. From Earth, Pluto's surface is seen with a very low resolution, and it is difficult to resolve spatial variations in ice composition. Measurements using Pluto's rotation have however allowed identification of surface compositional heterogeneities [*Grundy et al.*, 2013; *Merlin*, 2015]. For instance, *Merlin* [2015] showed that Pluto's spectra are well explained when considering two different areas, one composed of at least 98% of N_2 with a small proportion of CH_4 and CO, and a second one composed of about 60–80% CH_4 and 20–40% of tholin, a complex hydrocarbon compound.

New Horizons spacecraft confirmed the heterogeneous spatial distribution of ices. In particular, according to *New Horizons* data, Sputnik Planitia is characterized by an enrichment of CO and CH_4 ices and a strong absorption of N_2 ice [*Grundy et al.*, 2016]. Because CH_4 ice is much lighter than N_2 ice [*Spencer and Moore*, 1992], Sputnik Planitia may have a thin surface layer composed of CH_4-dominated ice and an interior of N_2/CO ice. The behavior of the three components in the mixture are however not known, and it is difficult to constrain the exact ice composition. Based on these different results, we follow previous studies on Sputnik Planitia dynamics [*McKinnon et al.*, 2016; *Trowbridge et al.*, 2016] and assume that Sputnik Planitia's glacier is composed of pure N_2 ice.

Properties of nitrogen ice vary with both temperature and pressure. Pluto's surface pressure is well constrained, ~10 μbar [*Yelle and Lunine*, 1989; *Sicardy et al.*, 2016; *Gladstone et al.*, 2016], and can be considered as zero when estimating Sputnik Planitia properties. The surface temperature has been constrained using the temperature dependence of the nitrogen absorption spectra. *Tryka et al.* [1994] obtained a temperature of 40 ± 2 K, a result confirmed by more recent studies [e.g., *Grundy et al.*, 2013; *Merlin*, 2015; *Stern et al.*, 2015]. Considering that the surface temperature is in vapor pressure equilibrium, *New Horizons* data suggest a surface temperature of 37 ± 3 K [*Gladstone et al.*, 2016]. In the following, we will assume a surface temperature of 37 K.

Table 1. Physical Properties of Sputnik Planitia Assuming a Pure Nitrogen Ice Composition at 37 K

Symbol	Name	Unit	Value	Reference	Assumed Value
ρ	Density	kg m^{-3}	1000	*Spencer and Moore* [1992]	1000
α	Thermal expansion	K^{-1}	2×10^{-3}	*Heberlein et al.* [1970]	2×10^{-3}
			2×10^{-3}	*Krupskii et al.* [1975]	
g	Acceleration of gravity	m s^{-2}	0.62	*Brozović et al.* [2015]	0.62
C_p	Heat capacity	J kg^{-1} K^{-1}	1350	*Scott* [1976]	1350
λ	Thermal conductivity	W m^{-1} K^{-1}	0.21	*Spencer and Moore* [1992]	0.25
			0.27	*Konstantinov et al.* [2005]	
κ	Thermal diffusivity	m^2 s^{-1}		$\kappa = \lambda/\rho C_p$	1.85×10^{-7}

The temperature dependence of nitrogen ice properties has been extensively studied [see *Scott*, 1976; *Manzhelii and Freiman*, 1997, and references therein]. In particular, the parameters influencing thermal convection within Sputnik Planitia are well constrained by laboratory measurements (Table 1), except for viscosity that must be extrapolated from experimental results, potentially introducing large uncertainties. *Yamashita et al.* [2010] studied the rheology of nitrogen ice for a temperature ranging from 5 K to 77 K and for a strain rate varying between 10^{-4} s^{-1} and 10^{-2} s^{-1}. Using these experimental results, *Trowbridge et al.* [2016] inferred that the viscosity variations caused by temperature variations across Sputnik Planitia would be about 1 order of magnitude, which can be considered as isoviscous. Alternatively, *McKinnon et al.* [2016] suggested that the viscosity contrast across Sputnik Planitia is between ~150 and 2×10^5. The large difference between these two studies is caused first by the different ΔT considered, 11 K for *Trowbridge et al.* [2016] and 27 K for *McKinnon et al.* [2016], and second by the fact that *McKinnon et al.* [2016] also considered the effect of the grain size and the activation energy for volume diffusion [*Estève and Sullivan*, 1981; *Eluszkiewicz*, 1991]. Overall, it is important to keep in mind that the uncertainties on the determination of the viscosity and its corresponding temperature variations are very large and should be taken with great care.

Another important parameter influencing the dynamics of Sputnik Planitia is its thickness. The exact ice layer thickness is, however, unknown. Assuming that Sputnik Planitia is located on a huge impact crater, as suggested by the formation mechanism proposed by *Bertrand and Forget* [2016], *Nimmo et al.* [2016] propose an upper bound of about 7 km based on impact craters on the Moon and Iapetus, while *Trowbridge et al.* [2016] suggest a minimum thickness of about 5 km in order to keep the observed icebergs afloat. On the basis of these estimates, we can only exclude ice layer thickness above 10 km. Following *McKinnon et al.* [2016], we consider a reference value of 4.5 km to rescale the dynamic topography and the size of polygons obtained in our simulations. The amplitude of the topography, varying in the range 20–40 km, and the size of polygons, up to 150 m, estimated from *New Horizons* images can be used to discriminate between different possible models of convection. Several sources of uncertainties may however affect the estimated amplitude of topography. For instance, a thin surface veneer of light elements (CH_4 and CO) may accumulate in the troughs. In addition, external processes, such as erosion and topographic instabilities, can substantially modify the topography [*McKinnon et al.*, 2016]. Overall, the shape and wavelength of the surface pattern is a better constraint than the amplitude of the topography.

3. Sputnik Planitia Dynamics: Insights From 3-D Cartesian Models of Convection

Previous studies of Sputnik Planitia dynamics considered either 2-D Cartesian models of convection [*McKinnon et al.*, 2016] or parameterized convection [*Moore et al.*, 2016; *Trowbridge et al.*, 2016] and, therefore, did not directly verify that the surface planform predicted by these models are consistent with the observed polygonal structures. In this section, we perform 3-D Cartesian models of convection for different setups, including different modes of heating and different rheologies, to identify the models that fit Sputnik Planitia observations at best. In particular, we focus on the influence of the mode of heating, basal or volumetric, on the surface pattern and topography.

Table 2. Numerical Simulations Used in This Study[a]

Source of Heating	Rayleigh Number	$\Delta\eta$	Grid Resolution	Aspect Ratio	BCs	Amplitude Topography
BH	10^5	0	$512 \times 512 \times 64$	16:16:1	FR	~30 m
BH	10^6	0	$512 \times 512 \times 64$	16:16:1	FR	~20 m
BH[b]	10^4	10^5	$128 \times 128 \times 64$	4:4:1	FF	~20 m
BH[c]	280	50	$512 \times 512 \times 64$	16:16:1	RR	~40 m
BH	750	400	384×64	12:1	FR	~70 m
BH	750	400	$512 \times 512 \times 64$	16:16:1	FR	~70 m
BH[c]	750	400	$512 \times 512 \times 64$	16:16:1	FR	~70 m
BH[c]	2800	50	$512 \times 512 \times 64$	16:16:1	RR	~45 m
VH[d]	$10^{4.7}$	0	$1024 \times 1024 \times 64$	16:16:1	FF	~50 m
VH[d]	$10^{5.15}$	0	$1024 \times 1024 \times 64$	16:16:1	FF	~80 m
VH[d]	$10^{5.5}$	0	$512 \times 512 \times 64$	6:6:1	FF	~100 m
VH	$10^{5.15}$	130	$1024 \times 1024 \times 64$	16:16:1	FF	~60 m
MH	$10^{5.64}$[e]	0	$512 \times 512 \times 64$	16:16:1	FR	~50 m
MH	$10^{5.2}$[f]	0	$512 \times 512 \times 64$	16:16:1	FR	~50 m

[a]BH stands for bottom heated convective systems, VH for volumetrically heated convective systems, and MH for both volumetrically and basally heated convective systems. The boundary conditions (BCs) are either free slip at top and bottom (FF) or free-slip top and rigid bottom (FR).
[b]*Deschamps and Lin* [2014].
[c]Nonuniform initial temperature condition.
[d]*Vilella and Kaminski* [2017].
[e]$Ra = 10^{4.6}$ and $H^* = 11$.
[f]$Ra = 10^{4.5}$ and $H^* = 5$.

3.1. Numerical Model

Numerical simulations presented in this work are either taken from previous studies [*Deschamps and Lin*, 2014; *Vilella and Kaminski*, 2017] or performed for this study. In all cases, simulations have been carried out using StagYY [*Tackley*, 2008], which solves the dimensionless conservation equations of mass, momentum, and energy. Lateral boundary conditions are reflecting, and the top and bottom surfaces can be either rigid or free slip. In the case of Sputnik Planitia, the use of 3-D Cartesian geometry is a good approximation, because the ice layer is much wider than high, and its curvature is therefore negligible. The thickness of Sputnik Planitia is not constrained by measurements, and therefore we do not know its exact aspect ratio. Grid resolution and aspect ratio of the numerical simulations we used vary in the ranges $128 \times 128 \times 64$ to $1024 \times 1024 \times 64$ and 4:4:1 to 16:16:1, respectively. In all cases, however, the lateral and radial resolutions are sufficient to correctly sample thermal boundary layers, plumes, and downwellings. All the cases discussed in this study are listed in Table 2.

The initial temperature condition is uniform with some random perturbations. Note that initial temperature conditions may influence the flow pattern [e.g., *White*, 1988]. We discuss these effects in section 5.1. We assume that the system reaches a steady or quasi-stationary state when its top heat flux and volume average temperature oscillate around constant values and when its pattern of convection does not substantially change with time. The main input of the numerical simulations is the Rayleigh number that quantifies the vigor of convection, convection being more vigorous with increasing Ra. In the case of bottom heating, the Rayleigh number is given by

$$Ra = \frac{\rho g \alpha \Delta T d^3}{\kappa \eta}, \tag{1}$$

where ρ is the density, g the acceleration of gravity, α the thermal expansion coefficient, ΔT the temperature jump across the fluid layer, d the layer thickness, η the dynamic viscosity, and $\kappa = \lambda / \rho C_p$ the thermal diffusivity, with λ the thermal conductivity, and C_p the heat capacity. In the case of volumetrically heated convection,

the temperature jump across the fluid layer is an output of the model and is therefore not known a priori. The temperature scale of the system (ΔT_H) is now related to the internal heating rate (H),

$$\Delta T_H = Hd^2/\lambda, \tag{2}$$

while the flow is controlled by the Rayleigh-Roberts number [*Roberts*, 1967],

$$Ra_H = \frac{\rho g \alpha \Delta T_H d^3}{\kappa \eta}. \tag{3}$$

In some cases, we consider a temperature-dependent viscosity following the Frank-Kamenetskii approximation, in which $\eta = \eta_0 \exp(-E(T-T_0)/RT_b^2)$, with η_0 the reference viscosity at the reference temperature T_0, E the activation energy, T the temperature, R the gas constant, and T_b the basal temperature. This rheology has been widely used to study stagnant-lid convection and is also considered by *McKinnon et al.* [2016] to model Sputnik Planitia dynamics. Due to variations in viscosity depending on the location, the Rayleigh number of a temperature-dependent viscosity system varies throughout the system. Because only the top temperature is well determined in both basal and volumetrically heated convection, we consider the surface Ra as the input of our numerical simulations.

An important output of our simulations is the dynamic topography (δh), which is obtained from the surface normal stress [*Hager and Richards*, 1989],

$$\delta h = \sigma_{zz}/\Delta \rho g, \tag{4}$$

where σ_{zz} is the component of the stress tensor normal to the surface, and $\Delta\rho$ the density jump at the interface. For an incompressible fluid, σ_{zz} writes

$$\sigma_{zz} = -P + 2\eta \frac{\partial V_z}{\partial z}, \tag{5}$$

with P the pressure and V_z the vertical velocity. The surface dynamic topography can therefore be expressed as

$$\delta h = \frac{1}{\rho g}\left(-P + 2\eta \frac{\partial V_z}{\partial z}\right). \tag{6}$$

StagYY calculates the dimensionless value of the dynamic topography, which can be rescaled with $\eta\kappa/\rho g d^2$. Note that, for bottom heated convection, $\eta\kappa/\rho g d^3 = \alpha \Delta T/Ra$, i.e., rescaling topography does not require the prescription of the surface viscosity, whose value is poorly known. The absolute topography of Sputnik Planitia is not known precisely, and depends on the reference surface topography for Pluto. We therefore set the average dynamic topography of our model to zero, and we focus on its pattern and peak-to-peak amplitude rather than on its absolute value.

3.2. Bottom Heated Convection for an Isoviscous Fluid

All previous studies on Sputnik Planitia's dynamics [*Moore et al.*, 2016; *McKinnon et al.*, 2016; *Trowbridge et al.*, 2016] assumed that the glacier is animated by Rayleigh-Bénard convection, for which the flow is driven by the heat flux at the bottom of the system. In the case of Sputnik Planitia, the heat available at the bottom of the glacier is generated by radioactive heating within Pluto's rocky core (and possibly its secular cooling) and transported by convection or conduction through the icy mantle to the surface. The convective system is organized in three parts: two thermal boundary layers (TBL), one at the top and one at the bottom, where temperature, and thus viscosity, changes sharply and heat is transported by conduction; and the convective interior, located between the two TBLs, and composed of active downwellings and upwellings. Figure 1a shows a typical horizontally averaged temperature profile for an isoviscous fluid. The separation of the system in three parts is underlined by the temperature change occurring within the two TBLs.

The Rayleigh number of the system depends on both the ice layer thickness and on the ice viscosity. For Sputnik Planitia, these two parameters are not well constrained, leading to large uncertainties in the Rayleigh number. To account for this uncertainty, *Trowbridge et al.* [2016] considered values of Ra between its critical value for the onset of convection, $Ra_{cr} \sim 10^3$, and 10^7. However, laboratory experiments showed that a polygonal pattern may be stable for Ra only in the range $10^5 - 10^6$ [*Busse and Whitehead*, 1971; *Whitehead and Parsons*, 1977; *White*, 1988]. Appropriate values of Ra for Sputnik Planitia should therefore range between 10^5 and 10^6.

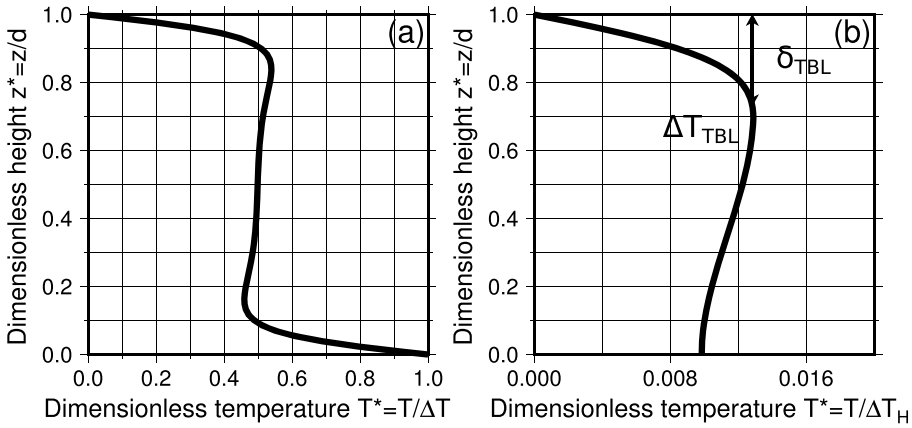

Figure 1. Typical horizontally averaged temperature profile of (a) bottom and (b) volumetrically heated convection obtained for $Ra = 10^5$ and $Ra_H = 10^{5.15}$, respectively. Both numerical simulations have free-slip top and bottom boundary conditions. The grid resolution and aspect ratio are $512 \times 512 \times 64$ and 8:8:1 for Figure 1a, and $1024 \times 1024 \times 64$ and 16:16:1 for Figure 1b. Height and temperature are dimensionless. The thermal boundary layer is characterized by its temperature jump (ΔT_{TBL}) and its thickness (δ_{TBL}).

Note that in laboratory experiments, the polygonal patterns are imposed as an initial condition; i.e., these experiments only show that polygonal patterns can remain stable for certain ranges of *Ra* and perturbations wavelength. Polygonal patterns are thus not necessarily the most stable pattern and may not necessarily be observed in natural systems. In particular, several other imposed patterns can remain stable for similar ranges of *Ra* and perturbations wavelength [*White*, 1988].

Figure 2 shows the surface temperature field and the dynamic topography of the convective system for $Ra = 10^5$ and $Ra = 10^6$. The numerical simulations have been conducted with a free slip top surface and a rigid bottom surface, which are the appropriate boundary conditions for Sputnik Planitia [*McKinnon et al.*, 2016].

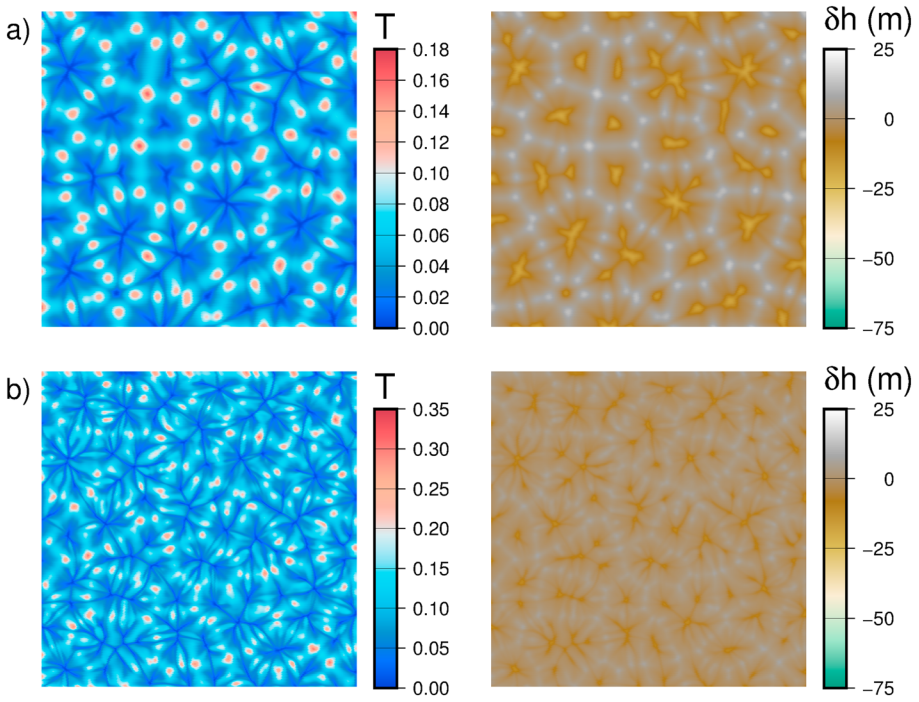

Figure 2. Subsurface temperature field (T in left column) and surface dynamic topography (δh in right column) of a bottom heated system conducted at (a) $Ra = 10^5$ and (b) $Ra = 10^6$. The top surface is free slip and the bottom one is rigid. The grid resolution is $512 \times 512 \times 64$ and the aspect ratio is 16:16:1. The temperature is dimensionless, while the dynamic topography is scaled with $d = 4.5$ km and $\Delta T = 20$ K.

The resulting dynamic topography is very different from the one observed on Sputnik Planitia. At $Ra = 10^5$, the surface planform is formed by narrow cylindrical upwellings and downwellings with, at least in some cases, a sheet-like shape. The downwellings, however, do not form a polygonal structure, while the upwellings do form a kind of polygonal structure, resulting in a topographic pattern opposite to the observed one. The observed topography may be caused by other processes occurring in upwellings, such as compaction or sublimation, but they are unlikely to produce a topography as large as the observed one. Furthermore, assuming a glacier's thickness of 4.5 km, the amplitude of the topography, around 30 m, is substantially lower than the estimated value for Sputnik Planitia [*Moore et al.*, 2016]. Fitting the observed amplitude, ~100 m, would require a very large ice layer thickness, around 15 km, which can be safely excluded (see section 2). At $Ra = 10^6$, the conclusions are similar, except that the polygonal structure formed by upwellings is much less clear and that the topography is even lower, around 20 m. Rayleigh-Bénard convection for an isoviscous fluid is therefore unlikely to produce a surface planform similar to that observed on Sputnik Planitia's surface.

3.3. Bottom Heated Convection in a Sluggish-Lid or Stagnant-Lid Regime

To account for the fact that nitrogen ice viscosity depends on temperature, *McKinnon et al.* [2016] run models with thermal viscosity contrasts $\Delta\eta$ in the range $100 - 10^5$. This range samples two distinct convective regimes [*Solomatov*, 1995], the sluggish-lid regime for $\Delta\eta < 10^4$, and the stagnant-lid regime for larger $\Delta\eta$. Interestingly, temperature-dependent viscosity is well known to affect the shape of the upwellings and downwellings, and in turn to change the surface planform.

To determine the dynamic topography for cases in the stagnant-lid regime, we used numerical simulations from *Deschamps and Lin* [2014], which include calculations with $\Delta\eta$ in the range $10^4 - 10^{10}$. Figure 3 shows the temperature field at two different depths (subsurface and dimensionless depth 0.35), and the surface dynamic topography for the case $Ra = 10^4$ and $\Delta\eta = 10^5$. Note that in this case the horizontal-to-vertical aspect ratio is equal to 4 and that the top and bottom boundaries are free slip. The temperature field at a dimensionless depth $d = 0.35$ has features similar to those found on Sputnik Planitia. In particular, we observe long sheets merging into Y junctions, which is the most common structure found on Sputnik Planitia. The size of the convective cell is about one fifth to one fourth the length of the box, i.e., comparable to the depth of the box. Applied to Sputnik Planitia, this implies an ice layer thickness of at least 20 km, which is, again, too large. In addition, the subsurface temperature field and the surface dynamic topography do not show a polygonal structure, and the amplitude of this topography is around 20 m, a very low value compared to Sputnik Planitia estimated topography [*Moore et al.*, 2016]. Changing the bottom boundary condition from free slip to rigid would affect the size of the convective cell, yielding more realistic ice layer thickness. However, it is unlikely to change the dynamic topography pattern or increase the amplitude of the topography [*Choblet and Parmentier*, 2009].

We then performed additional numerical simulations with small ($<10^3$) viscosity contrasts (sluggish-lid regime), which are more appropriate than the stagnant-lid regime to describe Sputnik Planitia [see also *McKinnon et al.*, 2016, section 2]. For these simulations, we imposed a free-slip mechanical boundary at the surface and a rigid boundary at the bottom. We first ran a case in 2-D Cartesian geometry similar to that in *McKinnon et al.* [2016] (Figures 4a and 4b) and found similar results. Note that the maximum and minimum values of the dynamic topography are different than those in *McKinnon et al.* [2016], simply because in our models we set the reference topography to its average value. The amplitude of topography is however similar. We then run a simulation in 3-D Cartesian geometry with exactly the same parameters as the 2-D Cartesian case (Figures 4c and 4d). For this 3-D Cartesian case, the subsurface temperature field is composed of wide cold donwellings forming large blobs surrounded by narrower hot upwellings that tend to assemble in sheets forming a polygonal structure. This result is similar to the one obtained by *Weinstein and Christensen* [1991] for a viscosity contrast of 50.6 and rigid boundary conditions. The resulting topography consists of a network of polygonal ridges (positive topography) surrounding troughs (negative topography). This is opposite to the topography observed at Sputnik Planitia, suggesting that convection within Sputnik Planitia does not operate in the bottom heated sluggish-lid regime. This result is consistent with the observation that temperature-dependent viscosity tends to produce narrower and faster plumes with a large head [*Farnetani and Richards*, 1994, 1995; *Kellogg and King*, 1997], whereas slabs, because of symmetry, tend to be wider and slower. Alternatively, positive topography triggered by upwellings may have been compensated either by sublimation, due to hotter local temperatures, or, in the case of Europa and Enceladus [*Nimmo et al.*, 2003; *Besserer et al.*, 2013], by temperature-dependent compaction of an initially porous ice layer. Upwellings would then be associated with negative topography. In the case of Sputnik Planitia, however, these scenarios seem unlikely. Sublimation of

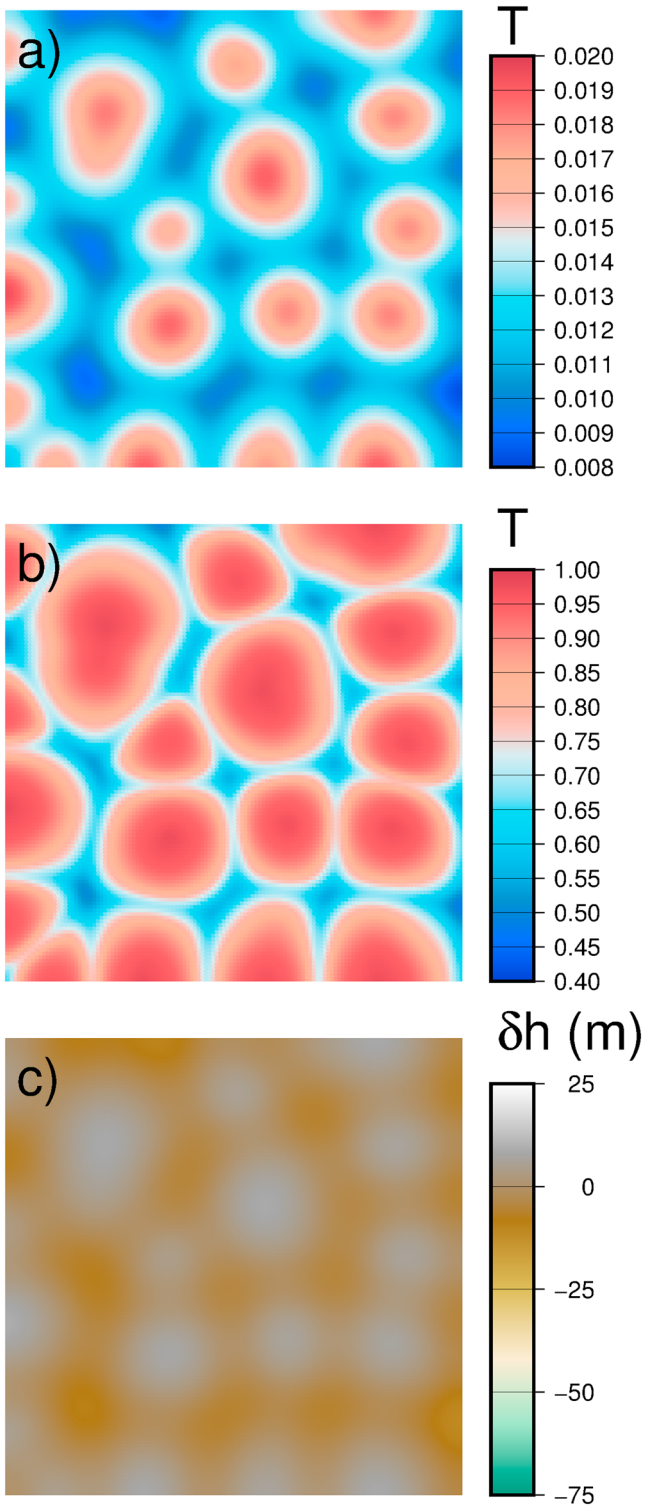

Figure 3. Temperature field, T, (a) at subsurface and (b) at $z = 0.65\,d$, and (c) surface dynamic topography, δh, obtained for a model from *Deschamps and Lin* [2014] conducted at $Ra = 10^4$, $\Delta\eta = 10^5$, and free-slip boundary conditions. The grid resolution is $128 \times 128 \times 64$ and the aspect ratio is 4:4:1. The temperature is dimensionless, while the dynamic topography is scaled with $d = 4.5$ km and $\Delta T = 20$ K.

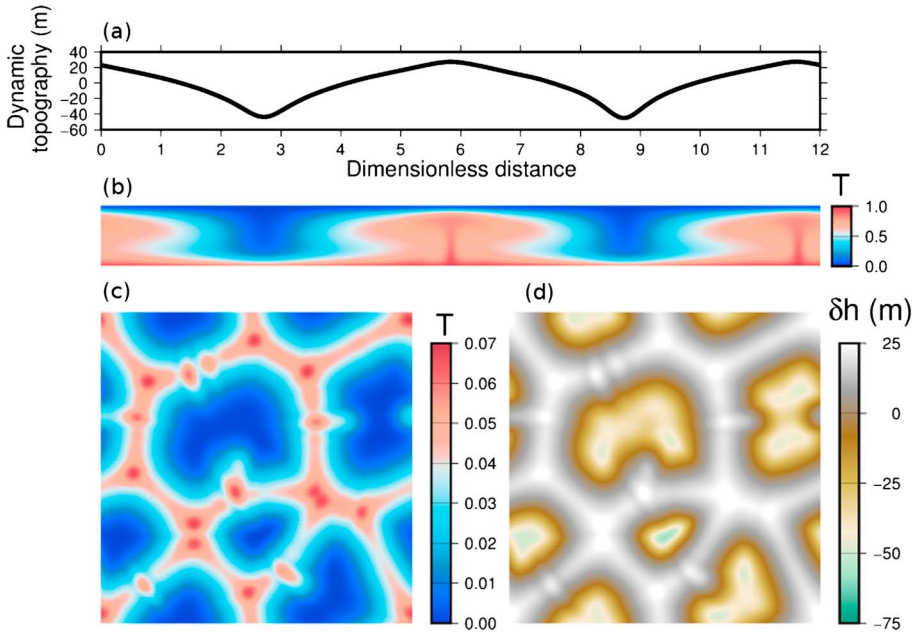

Figure 4. (a) Temperature field and (b) surface dynamic topography of a 2-D numerical simulation of a bottom heated system conducted at $Ra = 750$ and $\Delta\eta = 400$. (c) The subsurface temperature field, T, and (d) the surface dynamic topography, δh, for a 3-D numerical simulation obtained with the same controlling parameters as those of the 2-D simulation. Both numerical simulations have a free slip surface and a rigid base. The numerical simulations follow closely the one presented by *McKinnon et al.* [2016]. The grid resolution and aspect ratio are 384×64 and 12:1 for the 2-D case, and $512 \times 512 \times 64$ and 16:16:1 for the 3-D case. The temperature is dimensionless, while the dynamic topography is scaled with $d = 4.5$ km and $\Delta T = 20$ K.

a large volume of ice would be required to create a 100 m trough instead of a 50 m ridge. According to the phase diagram of nitrogen [*Manzhelii and Freiman*, 1997], this would in turn require relatively large temperatures at ~150 m depth, typically in excess of ~30 K compared to surface temperature, which is too large [see also *McKinnon et al.*, 2016, section 4]. Second, maintaining a negative topography of ~100 m by compaction over long time scale requires relatively strong lateral viscosity (and therefore, temperature) variations within the conductive part of the ice layer [*Nimmo et al.*, 2003; *Besserer et al.*, 2013]. By contrast, sluggish-lid convection operates for viscosity ratios lower than 10^3. This would allow maintaining compaction-induced topography only during a relatively short time (typically less than 10^4 years).

In order to obtain a surface planform dominated by a network of downwelling sheets leading to negative topography such as the one seen at the surface of Sputnik Planitia, the convective system should include ingredients favoring cold downwellings over hot upwellings, such as volumetric heating. The addition of internal heating in the convective system tends to lower the bottom heat flux [*Sotin and Labrosse*, 1999; *Deschamps et al.*, 2010], and in turn lower the influence of hot upwellings.

3.4. Volumetrically Heated Convection

In natural convecting systems, an alternative mode of heating is volumetric heating, in which the system is heated from within and cooled from the top. Common sources of volumetric heating are the decay of radioactive isotopes and tidal heating. Volumetric heating convection may further result from secular cooling, which can be formally treated as a source of volumetric heating [*Krishnamurti*, 1968; *Daly*, 1980; *Weinstein and Olson*, 1990]. A volumetrically heated convecting system is organized in two parts: a top TBL, and the convective interior composed of downwelling instabilities and nonbuoyant upwellings (return flow). Because the heat flux is fixed to zero at each point of the base of the fluid, there is no bottom TBL; i.e., thermal instabilities cannot form and generate thermal upwellings. Figure 1b shows a typical horizontally averaged temperature profile for an isoviscous, volumetrically heated fluid. The horizontally averaged temperature profile indicates that the thermal structure of the TBL, i.e., its temperature jump (ΔT_{TBL}) and thickness (δ_{TBL}), provides, at first order, the thermal structure of the whole system.

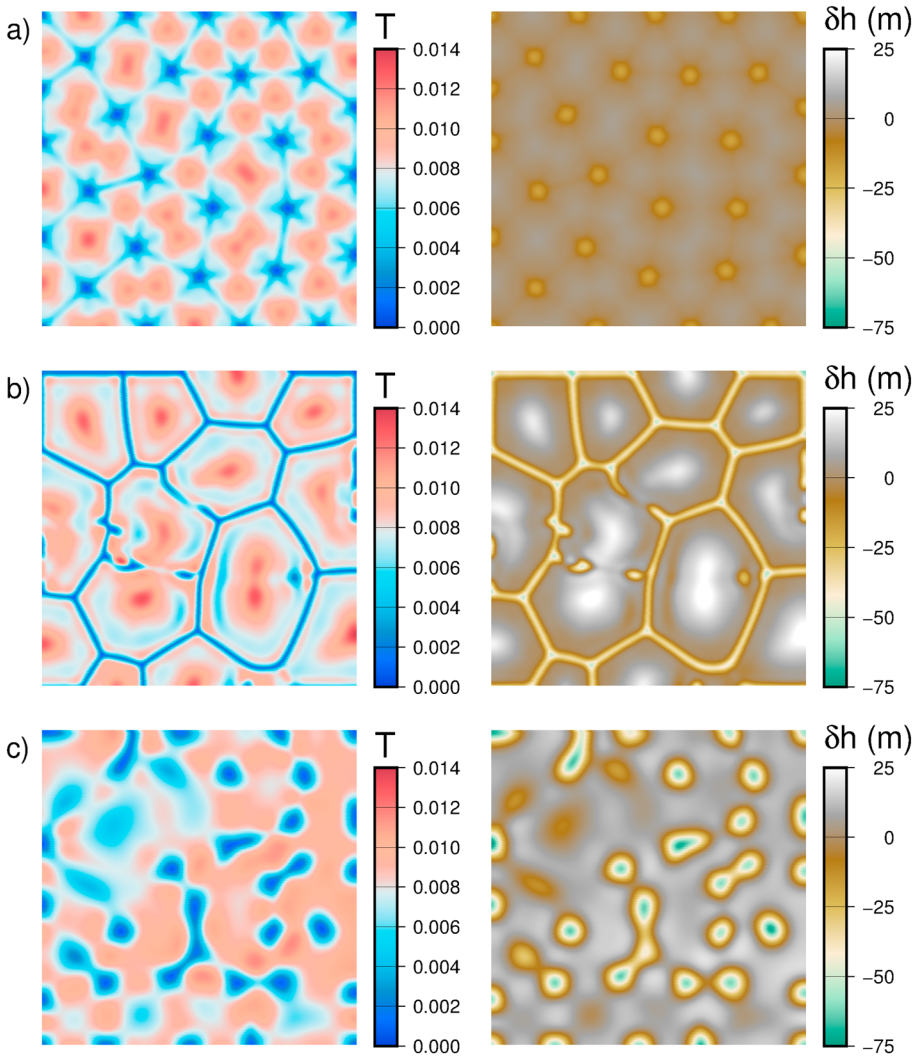

Figure 5. Subsurface temperature field, T, (left column) and surface dynamic topography, δh, (right column) of a volumetric heating system obtained for an isoviscous fluid and free slip boundary conditions, and conducted at (a) $Ra_H = 10^{4.7}$, (b) $Ra_H = 10^{5.15}$, and (c) $Ra_H = 10^{5.5}$. For Figures 5a and 5b, the grid resolution is $1024 \times 1024 \times 64$ and the aspect ratio is 16:16:1. For Figure 5c, the grid resolution is $512 \times 512 \times 64$ and the aspect ratio is 6:6:1. The temperature is dimensionless, while the dynamic topography is scaled with $d = 4.5$ km and a surface viscosity of 10^{15}Pa s.

Vilella and Kaminski [2017] conducted 3-D numerical simulations of volumetrically heated convection for an isoviscous fluid and both free-slip and rigid boundary conditions. Interestingly, these numerical experiments showed that changing the bottom boundary condition does not substantially affect the top thermal boundary layer, implying that surface topography for simulations conducted with a rigid bottom boundary condition are equivalent to those obtained with a free-slip boundary condition. We therefore consider, in all this section, a convective system with free slip boundary conditions. Calculations of *Vilella and Kaminski* [2017] further show that for Rayleigh-Roberts number (Ra_H, equation (3)) in the range 10^5 to $10^{5.5}$, the flow follows a sheet-like structure, in which long cold downwelling sheets merge in Y junctions, forming polygonal structures similar to those observed at Sputnik Planitia. By contrast, at $Ra_H < 10^5$, the flow is organized in squares or spokes patterns, while for $Ra_H > 10^{5.5}$, it consists of transient, irregular patterns.

Figure 5 shows maps of the subsurface temperature and of the dynamic topography for different values of Ra_H. Note that for Figure 5c the aspect ratio is equal to 6, which is lower than for Figures 5a and 5b where it equals 16. At $Ra_H = 10^{4.7}$, corresponding to the spokes pattern, dynamic topography is composed of a network of cylindrical depressions and slightly raised surrounding. The pattern of the dynamic topography does not form a polygonal structure, and the amplitude is small, around 50 m. This remains valid for $Ra_H < 10^{4.7}$.

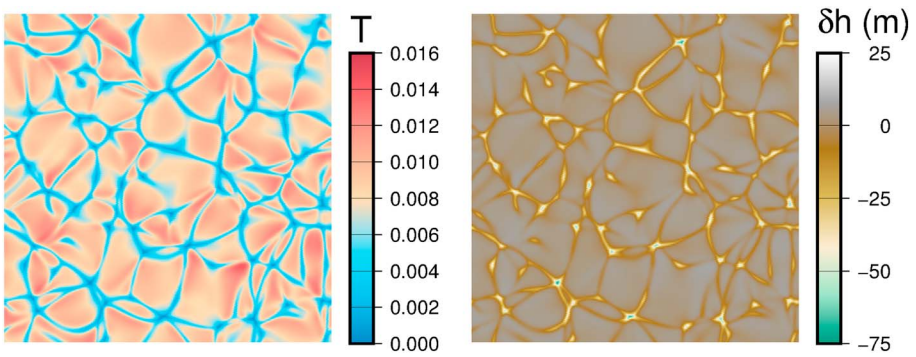

Figure 6. (left) Subsurface temperature field, T, and (right) surface dynamic topography, δh, of a volumetric heating system obtained for free slip boundary conditions and conducted at $Ra_H = 10^{5.15}$ and $\Delta\eta = 130$. The grid resolution is $1024 \times 1024 \times 64$ and the aspect ratio is 16:16:1. The temperature is dimensionless, while the dynamic topography is scaled with $d = 4.5$ km and a surface viscosity of 10^{15} Pa s.

For $Ra_H > 10^{5.5}$, corresponding to transient cases, dynamic topography consists in a network of depressions with irregular shapes and spacing, which, again, do not match the polygonal pattern observed at Sputnik Planitia. The topographic amplitude is much larger than that for $Ra_H < 10^{4.7}$, around 100 m. Again, these results remain valid for $Ra_H > 10^{5.5}$. At $Ra_H = 10^{5.15}$, corresponding to the sheet-like structure, dynamic topography has features very similar to those found on Sputnik Planitia. We observe long sheets merging into Y junctions, which is the most common structure found on Sputnik Planitia. Furthermore, the size of the convective polygonal cells is about 6 times the box depth, implying a thickness of Sputnik Planitia of about 3–4 km. Finally, the amplitude of the topography is around 80 m, i.e., in good agreement with the observations.

We also perform additional numerical simulations with temperature-dependent viscosity. Note that for this convective system the temperature jump across the fluid layer is a function of Ra_H, and therefore the viscosity jump is an output of the model. Figure 6 shows maps of the subsurface temperature and of the dynamic topography for $Ra_H = 10^{5.15}$ and $\Delta\eta = 130$. The results found in the isoviscous case remains valid in the sluggish-lid regime. In particular, the polygonal structure is still present, although less regular than in the isoviscous case. The topographic amplitude is about 60 m, which is slightly lower than in the isoviscous case. It should be noted, however, that the size of the convective polygonal cells is small compared to those observed for an isoviscous fluid (Figure 5b). To match the size of the polygonal patterns observed at the surface of Sputnik Planitia, and given the aspect ratio of our calculation (16:16:1), this implies a thickness of Sputnik Planitia of about 6–7 km, which in turn leads to a lower amplitude of the dynamic topography. In order to match simultaneously the size of the polygonal patterns and the amplitude of the topography, the increase of the thickness of Sputnik Planitia should be balanced by an increase in viscosity. Note that the value of the Rayleigh number can be maintained by changing the value of the internal heating rate. Because of large uncertainties on viscosity, internal heating rate, and ice layer thickness, the amplitude of the topography is not a strong constraint for a volumetrically heated system. A volumetrically heated system in a sluggish-lid regime can therefore explain the polygonal structure found on Sputnik Planitia, provided that the glacier is thick enough. It should further be pointed out that the Rayleigh number we used for the simulation plotted in Figure 6 is a surface Rayleigh number. The effective Rayleigh number, which is defined as the Rayleigh number at average temperature and viscosity of the convective interior and may be more representative of the convective vigor, is larger, around 10^7. Using smaller values of the surface Ra_H, would lead to smaller effective Ra_H, and may result in surface pattern with larger polygons. More generally, the surface pattern as a function of the Rayleigh number and the viscosity contrast for a volumetrically heated system still needs to be explored in detail.

Overall, the results from this section indicate that, for the range of parameters relevant to Sputnik Planitia, bottom heated convection fails to explain the polygonal structure observed at the surface of Sputnik Planitia. By contrast, volumetrically heated convection predicts pattern and dynamic topography that are consistent with these observations. A difficulty, however, is that no suitable source of internal heating within Sputnik Planitia has been identified so far. The most likely source is secular cooling, but it remains uncertain. We discuss this point in more detail in section 5. Despite this difficulty, in the next section we further explore implications of volumetrically heated convection using appropriate scaling laws.

4. Sputnik Planitia as a Volumetrically Heated System

Many studies addressing volumetrically heated convection have established scaling laws linking the thermal structure of the system to its Rayleigh number [*Parmentier and Sotin*, 2000; *Deschamps et al.*, 2012; *Limare et al.*, 2015; *Vilella and Kaminski*, 2017]. More specifically, the thickness of the TBL (δ_{TBL}) and its temperature jump (ΔT_{TBL}) are expressed as a power law of Ra_H,

$$\Delta T_{\mathrm{TBL}} = C_T \, \Delta T_H \, Ra_H^{\beta_T}, \tag{7}$$

$$\delta_{\mathrm{TBL}} = C_\delta \, d \, Ra_H^{\beta_\delta}, \tag{8}$$

where C_T, β_T, C_δ, and β_δ are dimensionless constants and ΔT_H and d the system temperature scale (equation (2)) and thickness, respectively. Thermal boundary layer analysis indicates that the exponents β_T and β_δ are both equal to $-1/4$ [*Jaupart and Mareschal*, 2011; *Deschamps et al.*, 2012], and numerical experiments match these values almost perfectly [*Parmentier and Sotin*, 2000; *Deschamps et al.*, 2012]. The two scaling constants, C_T and C_δ, are commonly obtained by fitting numerical or experimental results and depend on the exact definition of the TBL (see *Vilella and Kaminski* [2017], for a detailed description). *Vilella and Kaminski* [2017] defined the thermal boundary layer using the temperature profile built from the maximum temperature at a given depth. This "hot temperature" profile enables visualizing the "critical" thermal boundary layer, i.e., the TBL just before thermal instabilities break off and sink. The resulting scaling laws are

$$\Delta T_{\mathrm{TBL}} = 0.5 \, \Delta T_H \, (Ra_{H,\mathrm{cr}}/Ra_H)^{1/4}, \tag{9}$$

$$\delta_{\mathrm{TBL}} = d \, (Ra_{H,\mathrm{cr}}/Ra_H)^{1/4}. \tag{10}$$

Importantly, the thickness of the TBL is a measured value and is not inferred from the temperature jump. The Rayleigh-Roberts number (equation (3)) also depends on the surface heat flux of the system (Hd), which, for volumetrically heated convection, is related to the amount of heat generated within the system. We can thus write

$$Hd = Ra_H \frac{\eta \lambda \kappa}{\rho g \alpha} d^{-4}, \tag{11}$$

which gives a direct relationship between the surface heat flux and the ice layer thickness.

Scaling laws give a full description of the thermal structure of the convective system as a function of Ra_H alone. The value of Ra_H being previously constrained between 10^5 and $10^{5.5}$, we can estimate the thermal structure of the system. Considering a temperature jump in the range 5–25 K and a surface viscosity of 10^{14}–10^{16} Pa s, our results indicate an ice layer thickness between 2 km and 10 km. Note that the temperature jump across the TBL is restricted to values below 25 K, imposed by the melting temperature of Nitrogen ice, i.e., 63 K [*Cheng et al.*, 1975], and the estimated surface temperature, ~37 K [*Gladstone et al.*, 2016]. These typical values lead to a surface heat flux ranging from 0.1 mW m^{-2} to 10 mW m^{-2}.

An additional and independent constraint on the ice layer thickness is provided by the troughs that separate the polygonal cells. If these troughs are the surface expression of cold downwellings such as those shown in Figure 5, their width, w_{obs}, should scale as the thickness of the thermal boundary layer [*Parmentier and Sotin*, 2000]. Using the scaling law in equation (10), for $Ra_H = 10^{5.25}$ and free-slip boundary conditions, the thickness of the thermal boundary layer is $\delta_{\mathrm{TBL}} = 0.264\, d$. Furthermore, a careful examination of the convection planform of our numerical simulations (Figure 5) indicates that the width of the descending sheets is about twice δ_{TBL}, i.e., $w_{\mathrm{obs}} = 0.528\, d$. The width of the observed troughs may thus be used to estimate the thickness of the glacier, following $d = 1.894\, w_{\mathrm{obs}}$. *Stern et al.* [2015] indicate that w_{obs} is ranging between 2 and 3 km, leading to a glacier's thickness between 3.8 and 5.7 km. However, this method has several possible sources of uncertainties. First, descending sheets do not all have the same size, and a better estimate would require the determination of an average w_{obs} over the entire surface of Sputnik Planitia together with a standard deviation, providing an estimate of the uncertainty. Second, the relationship $w_{\mathrm{obs}} = 2\, \delta_{\mathrm{TBL}}$ is empirical and may exhibit small fluctuations. Finally, the observed width of the troughs may be biased by surface processes, such as overlying deposits of material, in which case our previous estimates would be underestimated. Overall, considering a

50% uncertainty on the initial results, leads to an ice layer thickness between 1.9 km and 8.5 km. Interestingly, this independent estimate agrees very well with our previous results and with previous estimates [*Trowbridge et al.*, 2016; *Nimmo et al.*, 2016].

Supposing that volumetric heating drives convection within Sputnik Planitia, we derived an estimation of the glacier's properties, e.g., thickness and surface heat flux. Our results do not differ significantly from the previous estimates based on bottom heated convection [*McKinnon et al.*, 2016; *Trowbridge et al.*, 2016]. It therefore suggests that the surface planform is the best constraint available on the interior structure and properties.

5. Discussion

In section 3, we showed that bottom heated convection does not result in surface polygonal patterns, as observed on Sputnik Planitia. Volumetrically heated convection, by contrast, can explain such patterns, and we investigated possible implications for Sputnik Planitia using scaling laws describing thermal boundary layer properties [*Vilella and Kaminski*, 2017]. A remaining problem, however, is to identify a suitable source of internal heating within Sputnik Planitia. As a first step, we explore the effects of initial temperature condition on the surface planform obtained in bottom heated convection.

5.1. Initial Condition and Surface Planform in Bottom Heated Convection

As shown in section 3, starting bottom heated convection with a uniform temperature condition does not produce a surface pattern in agreement with the polygonal cells observed on Sputnik Planitia. Previous studies have however found that different planforms are stable, including a hexagonal pattern, at given control parameters (for early works, see *Busse* [1967] and *Busse and Whitehead* [1971]). Some patterns can only be obtained when a specific initial temperature condition is prescribed. For example, the laboratory experiments of *White* [1988], conducted with a temperature-dependent viscosity fluid, suggest that a hexagonal pattern is stable when the initial pattern of temperature varies with a specific wavelength. One may wonder whether selecting a specific initial condition in a bottom heated system is a plausible mechanism to explain the polygonal pattern on Sputnik Planitia. We now further investigate this possibility.

White [1988] found that the stability of the hexagon pattern only slightly depends on the value of the viscosity contrast, as long as the viscosity contrast is larger than ~20. Therefore, we first tested a model with a viscosity contrast of 50 and a surface Rayleigh number of 280. For these conditions, *Christensen and Harder* [1991] showed, using numerical simulations with small aspect ratio (2.4:1.4:1 to 4:4:1), that the hexagonal pattern is stable. We followed closely the model of *Christensen and Harder* [1991] except that we consider a large aspect ratio (16:16:1) and different wavelengths for the initial hexagonal pattern. Note that we used rigid top and bottom boundary conditions. Figure 7 (left column) shows the time evolution of the system until reaching a steady state. As predicted by *White* [1988] and *Christensen and Harder* [1991], we obtain a hexagonal network of cold downwellings. This pattern, however, is very different from the one observed on Sputnik Planitia. In particular, cells have more regular shape and are smaller. The typical size of the convective cell, about one eighth the length of the box, implies an ice layer thickness of about 15 km. The dynamic topography is characterized by narrow positive anomaly, and the total amplitude of about 40 m is lower than the observed one. These disagreements may be solved by changing the shape of the initial temperature condition. We thus conducted different numerical simulations with different types of initial temperature condition (triangle or hexagon) and different wavelengths. The resulting planforms do not differ significantly from the one shown in Figure 7 (left column), i.e., they cannot explain the polygonal network observed on Sputnik Planitia.

A number of parameters, including the Rayleigh number, may change significantly the resulting planform of convection. We conducted a numerical simulation with a higher-surface Rayleigh number, $Ra = 2800$ (Figure 7, middle column). In this case, we observe that the initial (imposed) hexagonal pattern first leads to a square pattern with some flaws, that later evolves toward a hexagonal pattern again. The change from a square pattern to a hexagonal pattern has been described by *White* [1988] and is found to be a major mechanism to form a hexagonal pattern. The final planform of convection obtained in our numerical simulation exhibits the coexistence of squares and hexagons. However, the planform of convection is still evolving, and small changes in the planform at a conductive time 20 and 53.4 can still be seen, indicating a very slow evolution. Because of this slow evolution, it seems difficult to obtain the final, or quasi-stationary, planform within a reasonable time. For similar reasons, it is unlikely that Sputnik Planitia has reached this final planform during its existence. Independent of this issue, the typical size of the convective cell, about one tenth the length of the box, implies an ice layer thickness of about 19 km, and an amplitude of the dynamic topography of

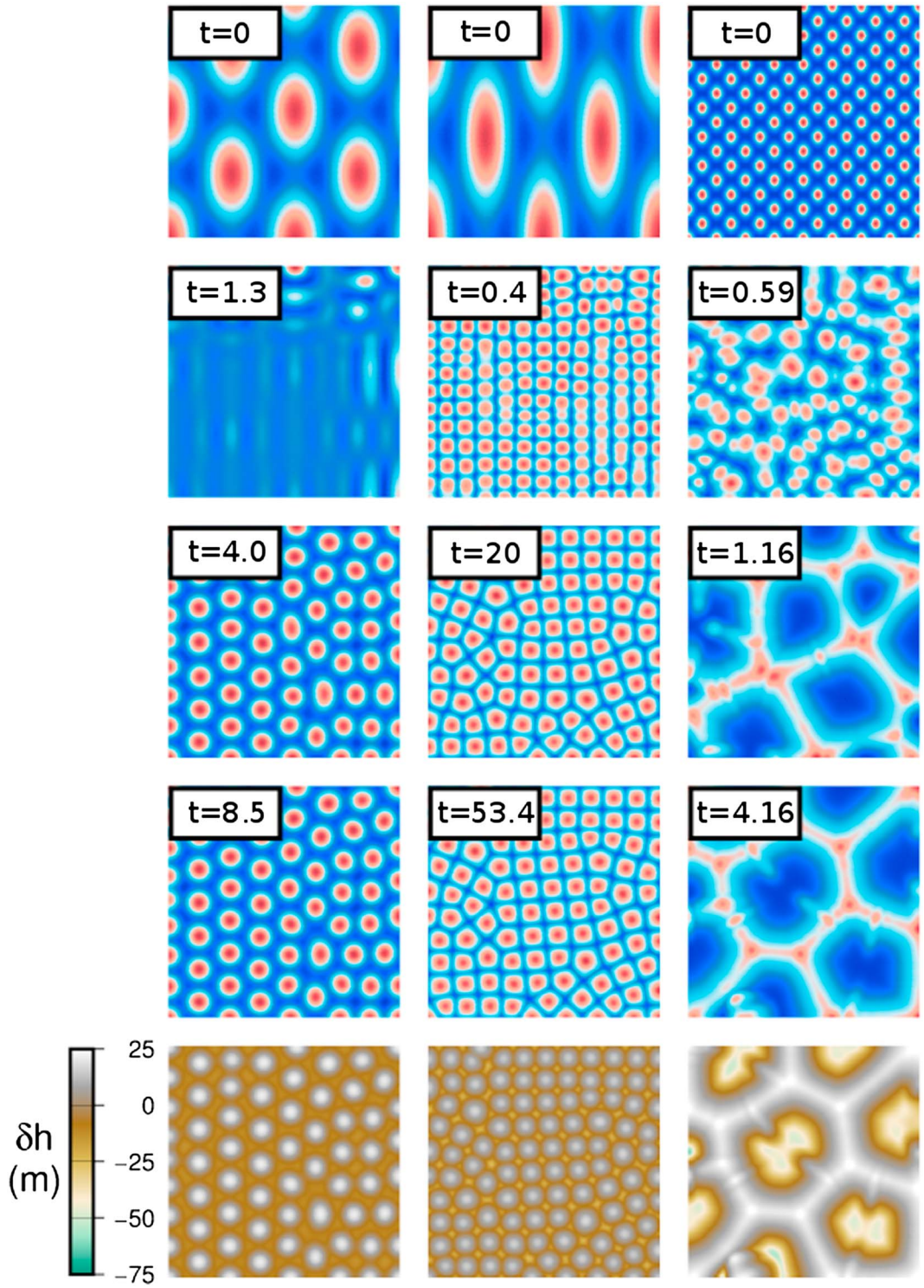

Figure 7. Subsurface temperature field, T, and surface dynamic topography, δh, of a bottom heated system taken at different conductive time t. Cases conducted for $\Delta\eta = 50$ and rigid boundary conditions with (left column) $Ra = 280$ and (middle column) $Ra = 2800$. (right column) Case conducted with the physical model used in Figure 4. For the three numerical simulations, the grid resolution is $512 \times 512 \times 64$ and the aspect ratio is 16:16:1.

about 45 m. Therefore, increasing the value of the surface Rayleigh number does not lead to a planform of convection explaining the polygonal pattern on Sputnik Planitia. In a second attempt, we considered the model developed in Figure 4 and proposed by *McKinnon et al.* [2016] with an initial temperature condition consisting of a hexagonal pattern with different wavelengths, from one half the length of the box to one tenth the length of the box. In all cases, we obtained the same planform of convection as that in Figures 4c and 4d. The numerical simulation with the lowest wavelength is presented in Figure 7 (right column). After a short transient regime, the planform of convection is clearly equivalent to the one obtained with a uniform initial temperature condition (Figures 4c and 4d).

We therefore conclude that even by imposing a specific initial condition, bottom heated convection does not produce a planform of convection explaining observations of Sputnik Planitia. Imposing a hexagonal pattern as initial condition enables to produce a polygonal pattern, but the wavelength of the polygonal pattern implies unrealistic ice layer thickness. It should further be emphasized that there is no apparent physical reason supporting the hypothesis that the initial temperature distribution of Sputnik Planitia followed a hexagonal pattern. While it is likely that the temperature field, just after the formation of Sputnik Planitia, was not uniform, it is difficult to justify a typical wavelength for temperature variations of about the size of the observed polygonal pattern. Moreover, because the defects may trigger the transition to another (more stable) convective pattern, the amount of defects in the initial condition affects strongly the stability of different patterns [*Cross and Hohenberg*, 1993].

5.2. Sources of Internal Heating

Purely volumetrically heated convection requires an internal source of heat. In the case of Sputnik Planitia, however, we could not identify a clear source of heat. Tidal heating may be safely ruled out. Rocks containing radiogenic elements may be embedded in the glacier and entrained by the flow, but their amount is certainly not large enough to produce the required heating. Similarly, viscous dissipation may be limited.

Because its effects are equivalent to internal heating [*Krishnamurti*, 1968; *Daly*, 1980; *Weinstein and Olson*, 1990], another possible source of heat in planetary bodies is secular cooling, i.e., the regular decrease of surface and internal temperature of the system. Note that this mechanism has been used to study volumetric heating in laboratory experiments [e.g., *Davaille and Jaupart*, 1993]. However, because condensation at the surface of Pluto occurs at the vapor pressure equilibrium temperature, it is unlikely that Sputnik Planitia's ice sheet condensed much warmer than ambient temperature, which may invalidate the hypothesis of secular cooling as a source of internal heating. Independently of the formation mechanism of Sputnik Planitia, the surface temperature of Pluto may vary with time over a long period of time, which would induce the cooling of Sputnik Planitia. In order to verify that secular cooling is a possible mechanism, it is important, first, to quantify the cooling rate required to explain the polygonal pattern, and second, to find a source of secular cooling with an appropriate cooling rate.

Assuming that the surface temperature of Sputnik Planitia is slightly colder than its interior, it is possible to estimate the cooling time as a function of the initial excess of temperature, ΔT_{prim}. The heat budget requires that the surface heat flux, Hd, is equal to the average cooling rate, which itself depends on the cooling time (t_c) and on its initial excess of temperature. Therefore,

$$H = \rho C_p \frac{\Delta T_{\text{prim}}}{t_c}. \tag{12}$$

The surface heat flux predicted by scaling laws built from numerical simulations of volumetrically heated convection ranges between 0.1 mW m^{-2} and 10 mW m^{-2} (section 4). Assuming an intermediate value of 4 mW m^{-2}, in agreement with the value used by *McKinnon et al.* [2016], for an ice layer thickness of 4.5 km and an initial excess of temperature $\Delta T_{\text{prim}} = 2$ K, the cooling time deduced from equation (12) is about 100 kyrs. The cooling of the glacier is thus slow enough to constitute a possible source of energy to maintain convection in Sputnik Planitia. It is also fast enough to explain the young estimated surface age of Sputnik Planitia [*Trilling*, 2016].

Periodic variations of the surface temperature, with period and amplitude large enough to affect the whole glacier, may provide a source of secular heating. When the surface temperature increases, the whole layer would be stable, and the interior temperature would increase by conduction. On the contrary, when the surface temperature decreases, convection would start again, and the interior temperature would decrease.

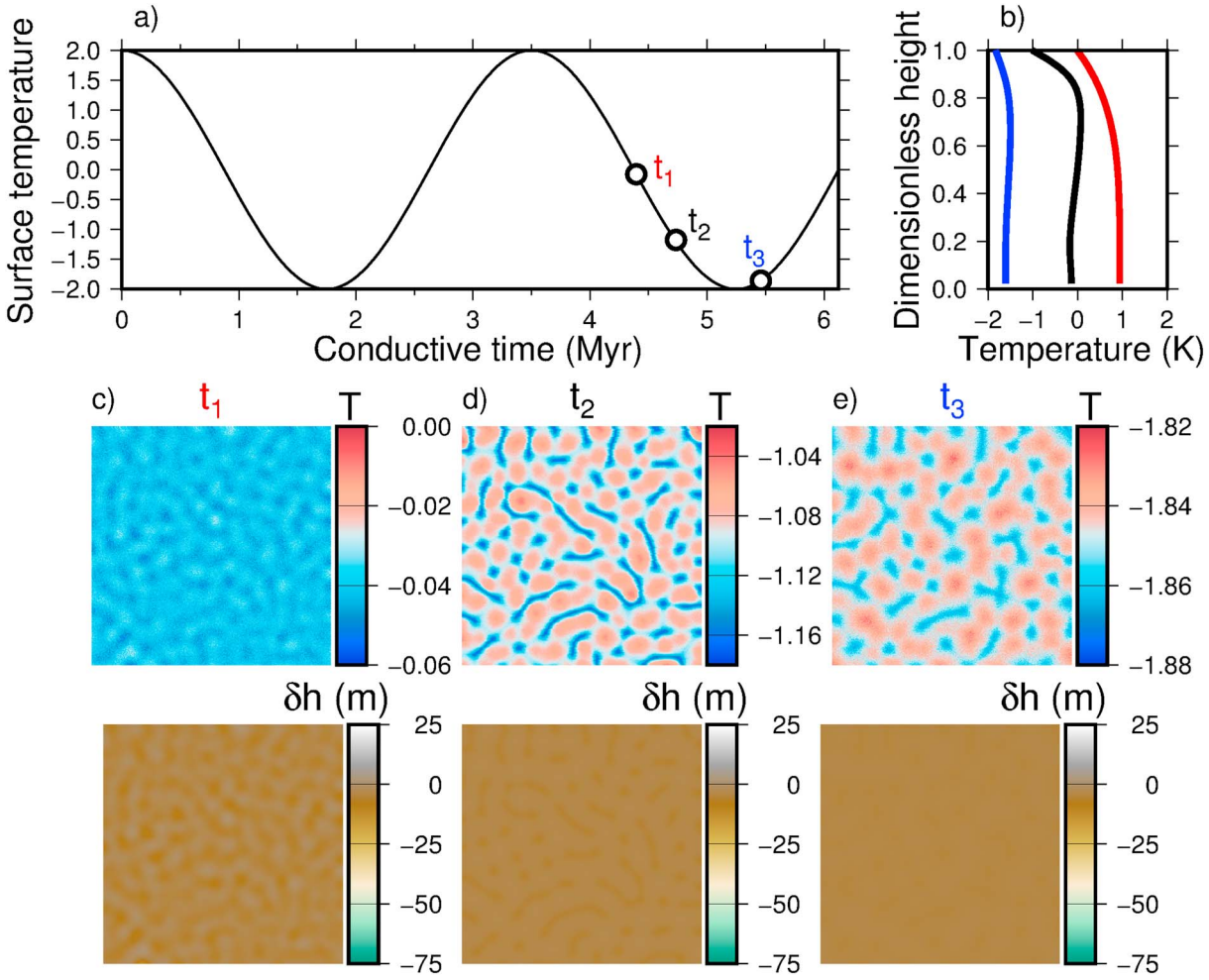

Figure 8. (a) Variations of surface temperature imposed in a numerical simulation conducted for $Ra = 10,000$ with a free slip surface and a rigid base. The conductive time is scaled with $t_{cond} = 3.5$ Myr corresponding to an ice layer thickness of about 4.5 km. (b) Horizontally averaged temperature profile at three different times shown in Figure 8a. (c–e) The subsurface temperature and corresponding surface dynamic topography field for the three specific times. The grid resolution is $512 \times 512 \times 64$ and the aspect ratio is 16:16:1. The dynamic topography is scaled with $d = 4.5$ km.

Again, this scenario requires the amplitude and period of the surface temperature variations to be in a specific range. Interestingly, calculation of Pluto's orbit over millions of years [*Williams and Benson*, 1971; *Dobrovolskis and Harris*, 1983; *Kinoshita and Nakai*, 1996] has shown a periodic variation with a time scale of 3–4 Myr, a number in agreement with the conductive time for a few kilometers thick glacier. Furthermore, *Earle et al.* [2017] have explored the possible effect of this orbital variation on the long-term surface temperature of Pluto, and found an important temperature variation at the north pole (4.3–7.5 K), and a more limited effect (1–3.5 K) in equatorial regions with higher albedo, such as Sputnik Planitia. Assuming a periodic variation of the surface temperature with an amplitude of 4 K, which is an extreme case, and a period equal to the conductive time $t_{cond} = d^2/\kappa$ for an ice layer thickness of about 4.5 km (i.e., ~3.5 Myr), we conducted a preliminary numerical simulation, with an adiabatic bottom surface and without internal heating. In this case, variations of surface temperature are the only source of heating. Note that we include small random perturbations of temperature at every time step in order to improve the convergence of the numerical code during the conductive period. Our results (Figure 8) indicate that variations in Pluto's orbit are able to trigger thermal convection within the glacier. The obtained planform of convection does not exhibit a polygonal structure, but is nevertheless typical of volumetric heating convection (compare Figures 5c and 8d), suggesting that a polyognal structure can be obtained with a different Rayleigh number. More importantly, the amplitude of the topography is small, ~5 m, and inconsistent with the observation of Sputnik Planitia. However, many parameters may modify the flow pattern, and their detailed influences need to be explored. These include (i) decreasing the surface viscosity, i.e., increasing *Ra*; (ii) including temperature-dependent viscosity; (iii) adding a small bottom

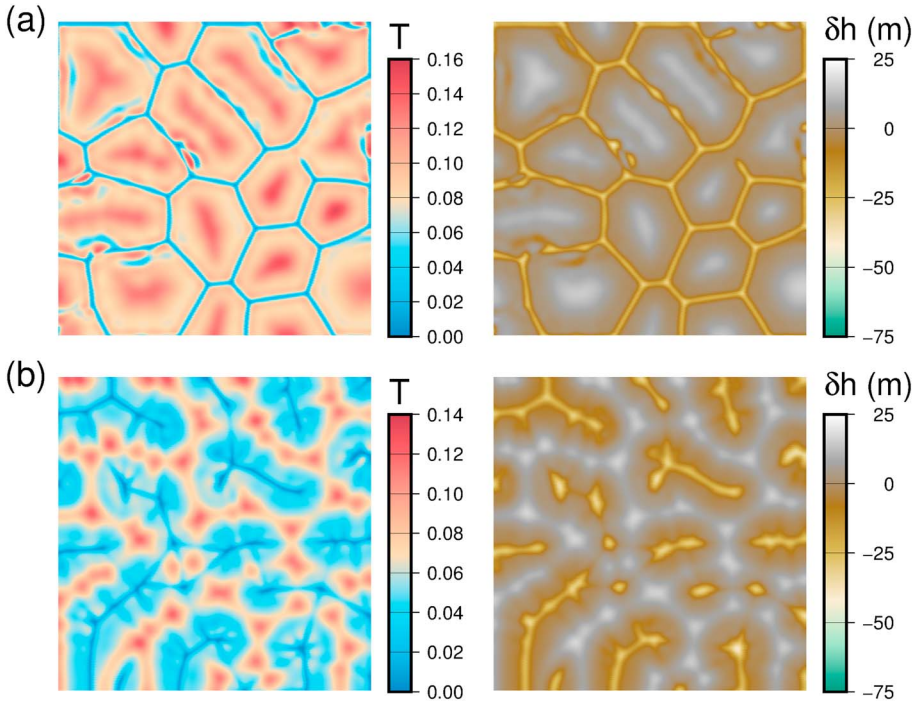

Figure 9. (left column) Subsurface temperature field, T, and (right column) surface dynamic topography, δh, of a system with both volumetric and bottom heating obtained for free slip boundary conditions and conducted at (a) $Ra = 10^{4.6}$ and $H^* = 11$ and (b) $Ra = 10^{4.5}$ and $H^* = 5$. For both numerical simulations the grid resolution is $512 \times 512 \times 64$ and the aspect ratio is 16:16:1. The temperature is dimensionless, while the dynamic topography is scaled with $d = 4.5$ km and $\Delta T = 20$ K.

heat flux (see section 5.3); and (iv) changing the ice layer thickness, i.e., increasing *Ra* and the conductive time. Investigating all these ingredients requires a large amount of computational time and is beyond the scope of this study.

5.3. Pluto's Internal Heat Flux and Mixed Heated Convection

Due to the decay of radioactive isotopes in Pluto's core, Pluto has internal heat flow [*Moore et al.*, 2016]. The exact value of the surface heat flux depends on physical properties of Pluto's interior, and on the mode of heat transfer through Pluto's icy mantle. For a 200 km thick mantle and a temperature jump of 200 K, and assuming a thermal conductivity of 2.6 W m^{-1} K^{-1} for water ice [*Hobbs*, 1974], the purely conductive heat flux is about 3 mW m^{-2}. If Pluto's ice mantle is still animated by convection, and using heat flux scalings from *Yao et al.* [2014], the surface heat flux may reach 10 mW m^{-2} [*Yao*, 2014]. Using a similar reasoning but different scalings, *Moore et al.* [2016] arrived at somewhat lower values, around 4.5 mW m^{-2}. It is important to note, however, that the crustal heat flux predicted by thermal evolution models of Pluto's interior is a horizontally averaged value. Surface heat flux may vary laterally and be locally much smaller than the average value. In absence of measurements, it is however impossible to make robust estimates of crustal heat flux beneath Sputnik Planitia.

In contrast to the volumetrically heated system, Sputnik Planitia has a bottom temperature fixed by the coupled evolution of Sputnik Planitia glacier and the underlying icy mantle. Therefore, Sputnik Planitia may be both volumetrically and basally heated. In that case, it may extract part of, but not necessarily all, the heat available at the top of the crust. The amount of heat that can be extracted from the crust and transported in the ice layer depends on the properties of this layer, in particular, on its amount of internal heating. If the amount of extracted heat is lower than the amount of crustal heat available from Pluto's interior, Sputnik Planitia would then act as an insulator, i.e., it may locally prevent the cooling of Pluto's crust.

A mixed heated system is controlled by two dimensionless parameters, the Rayleigh number equation (1) and the dimensionless internal heating rate,

$$H^* = \frac{Hd^2}{k\Delta T}. \tag{13}$$

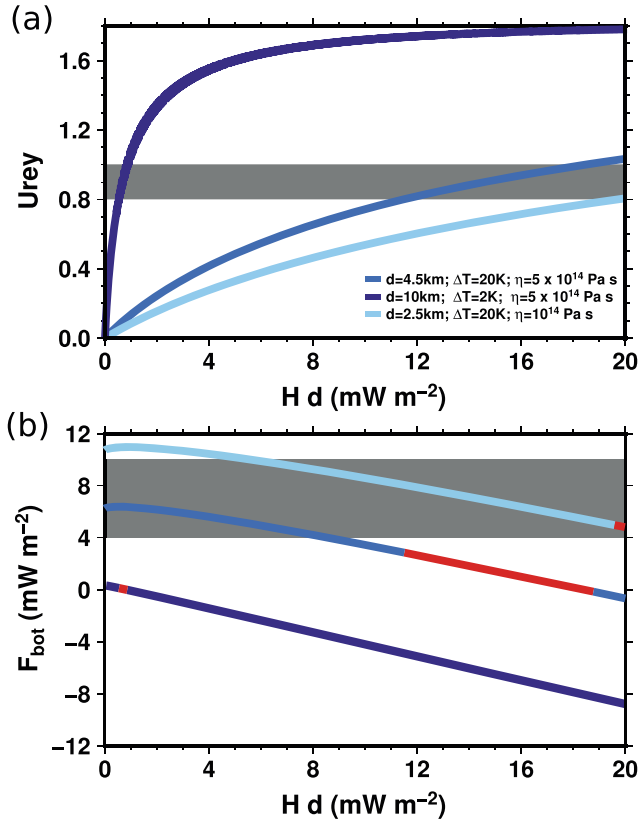

Figure 10. (a) Urey number (*Ur*) and (b) basal heat flux (F_{bot}) of the ice layer as a function of the heat flux due to internal heating (*Hd*), calculated for a system with both bottom and internal heating [*Deschamps et al.*, 2010]. Different values of ice layer thickness, viscosity, and temperature difference across the system are considered. The light grey shaded area corresponds to Urey numbers between 0.8 and 1, the conditions satisfying this constraint are shown in Figure 10b with the red portions of curves.

Constraining the stability domain of the sheet-like structure for this convective system requires a large set of numerical simulations, and is beyond the scope of this study. As a first insight, we focus on representative cases to check whether the sheet-like structure can be obtained in mixed heating convection. Figure 9a shows the subsurface temperature and dynamic topography obtained for $Ra = 10^{4.6}$ and $H^* = 11$, where 95% of the heat is generated within the system and 5% is coming from the bottom. In that case, we observe a sheet-like structure very similar to that obtained in the purely volumetric heating case. Note that the aspect ratio of the convective cells as well as the amplitude of the dynamic topography is slightly lower, implying a higher thickness of the glacier, about 5–7 km. Figure 9b shows the subsurface temperature and dynamic topography obtained for $Ra = 10^{4.5}$ and $H^* = 5$, where only 68% of the heat is generated within the system. We found that when the proportion of heat coming from the bottom increases, the downwelling instabilities are preferentially organized in straight lines, and the sheet-like structure is no longer observed. These results suggest that the addition of a small heat flux coming from the bottom of the system would not change the main conclusion drawn for the purely volumetrically heated case, provided that the internal heat source is significantly larger than the heat coming from the bottom. We now further quantify this effect.

The surface heat flux (F_{surf}) of the system is equal to the sum of the basal heat flux (F_{bot}) and the internal heat flux (*Hd*). The relative importance of the internal heat flux is measured with the Urey number,

$$Ur = \frac{Hd}{F_{surf}}, \tag{14}$$

where $Ur = 0$ indicates a system heated at its bottom only, $Ur = 1$ a purely internally heated system, and $Ur > 1$ a system where the heat internally generated flows from both the top and bottom boundaries. According to our few simulations for mixed heated fluids, sheet-like structure may appear for models with a Urey ratio close to one, typically in the range 0.8–1.0. Fixing a more accurate range however requires a systematic

study. Nevertheless, large Urey ratios imply that the amount of heat that can be extracted from the crust and transported toward the surface is limited. *Deschamps et al.* [2010] have established scaling laws linking F_{surf} to the two dimensionless numbers of the system,

$$F_{surf} = 0.52 \frac{k\Delta T}{d} Ra^{0.306} \theta_H^{4/3}, \quad (15)$$

where,

$$\theta_H = 0.5 + 0.88\, h^{0.779}\, Ra^{-0.234} \quad (16)$$

is the volume average temperature of the system. Figure 10a plots the Urey number as a function of the heat flux due to internally generated heat (*Hd*) for different values of the ice layer thickness, temperature difference, and viscosity. Our results indicate that the condition $Ur > 0.8$, required to obtain surface polygonal patterns in the mixed heating case, can be satisfied for reasonable parameter values. Note that relationships 15 and 16 were obtained for free-slip boundary conditions at both the top and the bottom of the system and that imposing a rigid base may induce small changes in these scaling laws. Figure 10b further shows that, for this range of *Ur*, the basal heat flux that can be accommodated by the glacier is always lower than the estimated crustal heat flux originating from Pluto's interior (grey band in Figure 10b). For instance, for $d = 4.5$ km, $\Delta T = 20$ K, and $\eta = 5 \times 10^{14}$ Pa s, the basal heat flux is lower than 2.8 mW m^{-2}. If mixed heating convection operates within Sputnik Planitia and is responsible for its surface polygonal patterns, Pluto's crust might therefore be locally warmer due to a blanketing effect induced by the glacier. Again, it should be kept in mind that the estimates of internal heat flux are horizontally averaged values and that the internal heat flux beneath Sputnik Planitia may be locally much lower and may thus be entirely or nearly entirely transferred to the surface.

6. Conclusion and Perspectives

We performed numerical simulations of Sputnik Planitia dynamics and found that bottom heated convection does not produce surface planforms consistent with those observed at the surface of Sputnik Planitia, whereas volumetrically heated convection does. The surface planforms predicted by our numerical models clearly indicate that, if Sputnik Planitia is animated by convection, the polygonal structure observed at its surface can be explained only if the heat-driving convection is purely internal or dominated by internal sources. Assuming that volumetrically heated convection operates within Sputnik Planitia, we found that for reasonable temperature contrasts (5–25 K) and nitrogen ice viscosities (10^{14}–10^{15} Pa s), the ice layer thickness is ranging between 2 km and 10 km and the surface heat flux between 0.1 mW m^{-2} and 10 mW m^{-2}. We could not identify a clear source of internal heating, but a preliminary numerical simulation indicates that long-period variations of Pluto's surface temperature, due to long-period variations of its orbital parameters, are able to maintain convection within Sputnik Planitia. Additional calculations are needed to determine whether there exist sets of parameters consistent with the estimated properties of this glacier, for which the surface pattern predicted by simulations agrees with that observed at Sputnik Planitia. The evolution of Sputnik Planitia at different time scales may further influence the internal dynamics of the system. Sublimation and condensation cycles, with period of a few 10^4 years, may trigger dramatic variations in the glacier thickness [*Bertrand and Forget*, 2016]. In addition, nitrogen may flow from the edges of the glacier inward and may deposit on Sputnik Planitia, which behaves as a cold trap [*Umurhan et al.*, 2017]. Such variations in thickness would make thermal convection harder to operate. Coupled models of thermal convection and seasonal variations of Sputnik Planitia should be performed to better understand the evolution and dynamics of this glacier.

Acknowledgments
We are grateful to two anonymous colleagues for their thorough and constructive reviews that helped us to produce a much improved paper. We also thank Sabine Stanley for her careful editorial handling of the manuscript. This research was funded by the Ministry of Science and Technology of Taiwan (MOST) grant 105-2116-M-001-017, Academia Sinica grant AS-102-CDA-M02, and TERRA-MWH project (ANR-11-ISO4-0004). Numerical computations were performed partly on IESAS Linux Cluster, and partly on the SCAPAD platform, IPGP. All the data used for generating the figures are available for academic purposes through the website of Academia Sinica (www.earth.sinica.edu.tw/~vilella/Materials_6.php).

References

Bertrand, T., and F. Forget (2016), Observed glacier and volatile distribution on Pluto from atmosphere topography processes, *Nature*, *540*, 86–89, doi:10.1038/nature19337.

Besserer, J., F. Nimmo, J. H. Roberts, and R. T. Pappalardo (2013), Convection-driven compaction as a possible origin of Enceladus's long wavelength topography, *J. Geophys. Res. Planets*, *118*, 908–915, doi:10.1002/jgre.20079.

Brozović, M., M. R. Showalter, R. A. Jacobson, and M. W. Buie (2015), The orbits and masses of satellites of Pluto, *Icarus*, *246*, 317–329, doi:10.1016/j.icarus.2014.03.015.

Busse, F. H. (1967), On the stability of two-dimensional convection in a layer heated from below, *J. Math. Phys.*, *46*, 140–150.

Busse, F. H., and J. A. Whitehead (1971), Instabilities of convection rolls in a high Prandtl number fluid, *J. Fluid Mech.*, *47*, 305–320, doi:10.1017/S002211207900015X.

Cheng, V. M., W. B. Daniels, and R. K. Crawford (1975), Melting parameters of methane and nitrogen from 0 to 10 kbar, *Phys. Rev. B*, *11*, 3972–3975, doi:10.1103/PhysRevB.11.3972.

Choblet, G., and E. M. Parmentier (2009), Thermal convection heated both volumetrically and from below: Implications for predictions of planetary evolution, *Phys. Earth Planet. Inter.*, *173*, 290–296, doi:10.1016/j.pepi.2009.01.005.
Christensen, U., and H. Harder (1991), 3-D convection with variable viscosity, *Geophys. J. Int.*, *104*, 213–226, doi:10.1111/j.1365-246X.1991.tb02505.x.
Cross, M. C., and P. C. Hohenberg (1993), Pattern formation outside of equilibrium, *Rev. Modern Phys.*, *65*(3), 851–1112.
Cruikshank, D. P., et al. (2015), The surface compositions of Pluto and Charon, *Icarus*, *246*, 82–92, doi:10.1016/j.icarus.2014.05.023.
Daly, S. F. (1980), Convection with decaying heat sources: Constant viscosity, *Geophys. J. R. Astron. Soc.*, *61*, 519–247, doi:10.1111/j.1365-246X.1980.tb04831.x.
Davaille, A., and C. Jaupart (1993), Transient high-Rayleigh-number thermal convection with large viscosity variation, *J. Fluid Mech.*, *253*, 141–166, doi:10.1017/S0022112093001740.
Deschamps, F., and J. R. Lin (2014), Stagnant lid convection in 3D-Cartesian geometry: Scaling laws and applications to icy moons and dwarf planets, *Phys. Earth Planet. Inter.*, *229*, 40–54, doi:10.1016/j.pepi.2014.01.002.
Deschamps, F., P. J. Tackley, and T. Nakagawa (2010), Temperature and heat flux scalings for isoviscous thermal convection in spherical geometry, *Geophys. J. Int.*, *182*, 137–154, doi:10.1111/j.1365-246X.2010.04637.x.
Deschamps, F., C. Yao, P. J. Tackley, and C. Sanchez-Valle (2012), High Rayleigh number thermal convection in volumetrically heated spherical shells, *J. Geophys. Res.*, *117*, E09006, doi:10.1029/2012JE004090.
Dobrovolskis, A. R., and A. W. Harris (1983), The obliquity of Pluto, *Icarus*, *55*, 231–235, doi:10.1016/0019-1035(83)90077-5.
Earle, A. M., R. P. Binzel, L. A. Young, S. A. Stern, K. Ennico, W. Grundy, C. B. Olkin, H. A. Weaver, the New Horizons Geology, and G. I. Tean (2017), Long-term surface temperature modeling of Pluto, *Icarus*, *287*, 37–46, doi:10.1016/j.icarus.2016.09.036.
Eluszkiewicz, J. A. (1991), On the microphysical state of the surface of Triton, *J. Geophys. Res.*, *96*, 19,217–19,229, doi:10.1029/91JA01858.
Estève, D., and N. S. Sullivan (1981), N.M.R. study of self-diffusion in solid N_2, *Solid State Commun.*, *39*, 969–671, doi:10.1016/0038-1098(81)90067-3.
Farnetani, C. G., and M. A. Richards (1994), Numerical investigation of the mantle plume initiation model for flood basalt events, *J. Geophys. Res.*, *99*, 13,813–13,883, doi:10.1029/94JB00649.
Farnetani, C. G., and M. A. Richards (1995), Thermal entrainment and melting in mantle plumes, *Earth Planet. Sci. Lett.*, *136*, 251–267, doi:10.1016/0012-821X(95)00158-9.
Gladstone, G. R., et al. (2016), The atmosphere of Pluto as observed by New Horizons, *Science*, *351*(6279), aad8866, doi:10.1126/science.aad8866.
Grundy, W. M., C. B. Olkin, L. A. Young, E. F. Buie, and M. W. Young (2013), Near-infrared spectral monitoring of Pluto's ices: Spatial distribution and secular evolution, *Icarus*, *223*, 710–721, doi:10.1016/j.icarus.2013.01.019.
Grundy, W. M., et al. (2016), Surface compositions across Pluto and Charon, *Science*, *351*(6279), aad9189, doi:10.1126/science.aad9189.
Hager, B. H., and M. A. Richards (1989), Long-wavelength variations in Earth's geoid: Physical models and dynamical implications, *Philos. Trans. R. Soc. A*, *328*, 309–327, doi:10.1098/rsta.1989.0038.
Heberlein, D. C., E. D. Adams, and T. A. Scott (1970), Thermal expansion and isothermal compressibility of solid nitrogen, *J. Low Temp. Phys.*, *2*, 449–463, doi:10.1007/BF00652513.
Hobbs, P. V. (1974), *Ice Physics*, Oxford Univ. Press, New York.
Jaupart, C., and J. C. Mareschal (2011), *Heat Generation and Transport in the Earth*, Cambridge Univ. Press, Cambridge, U. K.
Kellogg, L. H., and S. D. King (1997), The effect of temperature dependent viscosity on the structure of new plumes in the mantle: Results of a finite element model in a spherical, axisymmetric shell, *Earth Planet. Sci. Lett.*, *148*, 13–26, doi:10.1016/S0012-821X(97)00025-3.
Kinoshita, H., and H. Nakai (1996), Long-term behavior of the motion of Pluto over 5.5 billion years, *Earth Moon Planets*, *72*, 165–173, doi:10.1007/BF00117514.
Konstantinov, V. A., V. G. Manzhelii, V. P. Revyakin, and V. V. Sagan (2005), Isochoric thermal conductivity of solid nitrogen, *Low Temp. Phys.*, *31*, 419–422, doi:10.1063/1.1925369.
Krishnamurti, R. (1968), Finite amplitude convection with changing mean temperature. Part 1. Theory, *J. Fluid Mech.*, *33*, 445–455, doi:10.1017/S0022112068001436.
Krupskii, I. N., A. I. Prokhvatilov, and A. I. Erenburg (1975), X-ray studies of structure and thermal expansion in solid N_2, *Soviet J. Low Temp. Phys.*, *1*, 178–182.
Limare, A., K. Vilella, E. Di Giuseppe, C. Farnetani, E. Kaminski, E. Surducan, V. Surducan, C. Neamtu, L. Fourel, and C. Jaupart (2015), Microwave-heating laboratory experiments for planetary mantle convection, *J. Fluid Mech.*, *1565*, 14–18, doi:10.1017/jfm.2015.347.
Manzhelii, V. G., and Y. A. Freiman (1997), *Physics of Cryocrystals*, AIP-Press, Woodbury.
McKinnon, W. B., et al. (2016), Convection in a volatile nitrogen-ice-rich layer drives Pluto's geological vigour, *Nature*, *534*, 82–85, doi:10.1038/nature18289.
Merlin, F. (2015), New constraints on the surface of Pluto, *Astron. Astrophys.*, *582*, A39, doi:10.1051/0004-6361/201526721.
Moore, J. M., et al. (2016), The geology of Pluto and Charon through the eyes of New Norizons, *Science*, *351*(6279), 1284–1293, doi:10.1126/science.aad7055.
Nimmo, F., R. T. Pappalardo, and B. Giese (2003), On the origins of band topography, Europa, *Icarus*, *166*, 21–32, doi:10.1016/j.icarus.2003.08.002.
Nimmo, F., et al. (2016), Reorientation of Sputnik Planitia implies a subsurface ocean on Pluto, *Nature*, *540*, 94–96, doi:10.1038/nature20148.
Parmentier, E. M., and C. Sotin (2000), Three-dimensional numerical experiments on thermal convection in a very viscous fluid: Implications for the dynamics of a thermal boundary layer at high Rayleigh number, *Phys. Fluids*, *12*, 609–617, doi:10.1063/1.870267.
Prokhvatilov, A. I., and L. D. Yantsevich (1983), X-ray investigation of the equilibrium phase diagram of CH_4–N_2 solid mixtures, *Soviet J. Low Temp. Phys.*, *9*, 94–98.
Roberts, P. H. (1967), Convection in horizontal layers with internal heat generation. Theory, *J. Fluid Mech.*, *30*, 33–49, doi:10.1017/S0022112067001284.
Scott, T. A. (1976), Solid and liquid nitrogen, *Phys. Rep.*, *27*, 89–157, doi:10.1016/0370-1573(76)90032-6.
Sicardy, B., et al. (2016), Pluto's atmosphere from the 2015 June 29 ground-based stellar occultation at the time of the new horizons flyby, *Astrophys. J. Lett.*, *819*, L38, doi:10.3847/2041-8205/819/2/L38.
Solomatov, V. S. (1995), Scaling of temperature- and stress-dependent viscosity convection, *Phys. Fluids*, *7*, 266–274, doi:10.1063/1.868624.
Sotin, C., and S. Labrosse (1999), Three-dimensional thermal convection in an iso-viscous, infinite Prandtl number fluid heated from within and from below: Applications to the transfer of heat through planetary mantles, *Phys. Earth Planet. Inter.*, *112*, 171–190, doi:10.1016/S0031-9201(99)00004-7.
Spencer, J. R., and J. M. Moore (1992), The influence of thermal inertia on temperatures and frost stability on Triton, *Icarus*, *99*, 261–272, doi:10.1016/0019-1035(92)90145-W.

Stern, S. A., et al. (2015), The Pluto system: Initial results from its exploration by new horizons, *Science*, *350*, aad1815, doi:10.1126/science.aad1815.
Tackley, P. J. (2008), Modelling compressible mantle convection with large viscosity contrasts in a three-dimensional spherical shell using the Yin-Yang grid, *Phys. Earth Planet. Inter.*, *171*, 7–18, doi:10.1016/j.pepi.2008.08.005.
Trilling, D. E. (2016), The surface age of Sputnik Planum, Pluto, Must be less than 10 million years, *PLOS ONE*, *11*, e0147386, doi:10.1371/journal.pone.0147386.
Trowbridge, A. J., H. J. Melosh, J. K. Steckloff, and A. M. Freed (2016), Vigorous convection as the explanation for Pluto's polygonal terrain, *Nature*, *534*, 79–81, doi:10.1038/nature18016.
Tryka, R. H., K. A. Brown, D. P. Cruikshank, T. C. Owen, T. R. Geballe, and C. Debergh (1994), Temperature of nitrogen ice on Pluto and its implications for flux measurements, *Icarus*, *112*, 513–527, doi:10.1006/icar.1994.1202.
Umurhan, O. M., et al. (2017), Modeling glacial flow on and onto Pluto's Sputnik Planitia, *Icarus*, *287*, 301–319, doi:10.1016/j.icarus.2017.01.017.
Vilella, K. (2015), Modélisation théorique et numérique de la convection thermique, applications aux manteaux planétaires, PhD thesis, Institut de Physique du Globe, Paris, France.
Vilella, K., and E. Kaminski (2017), Fully determined scaling laws for volumetrically heated convective systems, a tool for assessing habitability of exoplanets, *Phys. Earth Planet. Inter.*, *266*, 18–28.
Weinstein, S. A., and P. Olson (1990), Planforms in thermal convection with internal heat sources at large Rayleigh and Prandtl numbers, *Geophys. Res. Lett.*, *3*, 239–242, doi:10.1029/GL017i003p00239.
Weinstein, S. A., and U. Christensen (1991), Convection planforms in a fluid with a temperature-dependent viscosity beneath a stress-free upper boundary, *Geophys. Res. Lett.*, *18*, 2035–2038, doi:10.1029/91GL02663.
White, D. B. (1988), The planforms and onset of convection with a temperature-dependent viscosity, *J. Fluid Mech.*, *191*, 247–286, doi:10.1017/S0022112088001582.
Whitehead, J. A., Jr., and B. Parsons (1977), Observations of convection at Rayleigh numbers up to 760,000 in a fluid with large Prandtl number, *Geophys. Astrophys. Fluid Dyn.*, *9*, 201–217, doi:10.1080/03091927708242327.
Williams, J. G., and G. S. Benson (1971), Resonances in the Neptune-Pluto system, *Astron. J.*, *76*, 167–176, doi:10.1086/111100.
Yamashita, Y., M. Kato, and M. Arakawa (2010), Experimental study on the rheological properties of polycrystalline solid nitrogen and methane: Implications for tectonic processes on Triton, *Icarus*, *207*, 972–977, doi:10.1016/j.icarus.2009.11.032.
Yao, C. (2014), The role of methanol on the evolution of icy bodies: Experimental and numerical approaches, PhD thesis, ETH Zurich, Zurich, Switzerland.
Yao, C., F. Deschamps, J. P. Lowman, C. Sanchez-Valle, and P. J. Tackley (2014), Stagnant lid convection in bottom-heated thin 3-D spherical shells: Influence of curvature and implications for dwarf planets and icy moons, *J. Geophys. Res. Planets*, *119*, 1895–1913, doi:10.1002/2014JE004653.
Yelle, R. V., and J. I. Lunine (1989), Evidence for a molecule heavier than methane in the atmosphere of Pluto, *Nature*, *339*, 288–290, doi:10.1038/339288a0.